Corrosion Science 64 (2012) 222–233

Contents lists available at SciVerse ScienceDirect

Corrosion Science

journal homepage: www.elsevier.com/locate/corsci

Mechanism of breakaway oxidation of Fe–Cr and Fe–Cr–Ni alloys in dry and wet carbon dioxide

Thomas Gheno [a,b], Daniel Monceau [a], David J. Young [b,*]

[a] Institut Carnot CIRIMAT, ENSIACET, 31030 Toulouse Cedex 4, France
[b] School of Materials Science and Engineering, The University of New South Wales, Sydney, NSW 2052, Australia

ARTICLE INFO

Article history:
Received 5 June 2012
Accepted 25 July 2012
Available online 7 August 2012

Keywords:
A. Steel
C. High temperature corrosion
C. Internal oxidation
C. Selective oxidation

ABSTRACT

Model Fe–Cr and Fe–Cr–Ni alloys were exposed to Ar–CO_2 and Ar–CO_2–H_2O gas mixtures at 650 °C. While all alloys initially formed protective Cr_2O_3 scales, nucleation and growth of iron-rich oxide nodules resulted in some cases in breakaway oxidation. The conditions leading to departure from the protective stage are discussed in terms of Cr_2O_3 thermodynamic and kinetic stability. The morphological and compositional evolutions accompanying nodule development were examined. The influence of carbide precipitation on alloy chromium diffusion and the ability of the alloy to form and maintain Cr-rich oxide layers was investigated.

1. Introduction

As part of the global effort to mitigate carbon dioxide emissions from coal-fired power plants, oxy-fuel combustion has emerged as a promising alternative to conventional technologies. As nitrogen is eliminated from the inlet gas, and coal is burnt in a mixture of oxygen and recirculated flue gas, the exhaust gas contains mainly CO_2 and H_2O, allowing easier separation of CO_2 for sequestration. The changed gas composition raises the question of fireside corrosion resistance of structural alloys in CO_2 + H_2O-rich atmospheres [1].

Ferritic and austenitic chromium-containing steels are used for various heat-resisting applications at moderate temperatures. However, Fe–Cr alloys are particularly prone to breakaway oxidation, defined as a rapid acceleration of the reaction rate. Breakaway is associated with the rapid growth of Fe-rich oxides on alloys initially forming protective Cr-rich oxide scales.

Commercial and model Fe–Cr materials which oxidise protectively in air have been shown to suffer breakaway oxidation in CO_2 [2–4]. The deleterious effect of CO_2 was related [2] to the extensive internal precipitation of chromium-rich carbides, which hinders the outward diffusion and selective oxidation of chromium.

Similarly, the addition of H_2O to a gas mixture, or its substitution for oxygen, is known to trigger breakaway oxidation of Fe–Cr alloys [5–9]. Various explanations of this effect have been proposed. Chromia scales have been shown to grow faster in the presence of H_2O [9–12], which has been attributed to hydrogen dissolution (in the form of OH^-) in the oxide [13]. The dissolution of hydrogen in the metal matrix is suggested to enhance internal oxidation of chromium, by increasing the permeability of oxygen [14]. In the presence of both oxygen and water vapour at moderate temperatures, formation of volatile species from Cr_2O_3 has been shown to enhance chromium depletion and trigger breakaway [4,15,16].

Recent studies [3,4] indicated that exposure of Fe–Cr alloys to CO_2–H_2O produced results similar to those observed in CO_2 or H_2O. The minimum chromium concentration required for Cr_2O_3 formation is increased by about the same amount in these atmospheres, over that required in air. The influence of alloy chromium concentration on the thermodynamic and kinetic stability of Cr_2O_3 has been studied [17,18], but a detailed description of the effect of CO_2 and H_2O is lacking. Furthermore, while the oxide morphology developed during the steady-state stage of non-selective oxidation in CO_2 and/or H_2O is well documented, and the corresponding reaction mechanism has been widely studied, little is known about the early-stage of Fe-rich oxide nodule formation in these environments. Mechanistic descriptions have been published for reaction in air at elevated temperatures (1000–1200 °C) [19,20], but the specific influence of CO_2 and H_2O is yet to be determined.

This paper is aimed at investigating the evolution of oxide morphology and composition during the transition from Cr_2O_3 to Fe-rich oxide formation during oxidation of Fe–Cr and Fe–Cr–Ni alloys in dry and wet CO_2 atmospheres at 650 °C.

2. Experimental

Binary and ternary alloys of composition given in Table 1 were prepared by argon arc melting Fe (99.99% pure), Cr (99.995% pure)

* Corresponding author. Tel.: +61 2 9385 4322; fax: +61 2 9385 5956.
E-mail address: d.young@unsw.edu.au (D.J. Young).

0010-938X/$ - see front matter © 2012 Elsevier Ltd. All rights reserved.
http://dx.doi.org/10.1016/j.corsci.2012.07.024

Table 1
Alloy composition (wt.%, base = Fe) and phase constitution (as annealed, determined by XRD).

Cr	Ni	
20		α
20	10	$\gamma-\alpha$
20	20	γ
25		α
25	10	$\gamma-\alpha$
25	20	γ

and Ni (99.95% pure). Ingots were annealed in Ar–5%H_2 at 1150 °C for 48 h, and cut into rectangular samples of approximate dimensions 14 × 6 × 1.5 mm. The phase constitution of annealed materials determined by XRD analysis is indicated in Table 1. The single phase alloys had coarse-grained (~500 μm) microstructures, while the two-phase alloys presented a finer (~10 μm) $\gamma-\alpha$ substructure. Specimens were mechanically ground to a 1200 grit finish, degreased and ultrasonically cleaned in ethanol before reaction.

Isothermal corrosion experiments were conducted at 650 °C in Ar–20%CO_2, Ar–20%CO_2–5%H_2O and Ar–20%CO_2–20%H_2O mixtures at a total pressure of about 1 atm. Linear gas flow rates were set at about 2 cm s^{-1}. The wet gases were generated by passing a mixture of Ar and CO_2 through a thermostatted water saturator. The distilled water in contact with the gas mixture was set at a temperature about 20 °C higher than that required to produce the nominal $p(H_2O)$. Excess water vapour was subsequently condensed by cooling the wet gas in a distillation column. Oxygen partial pressures in these mixtures are so low (~1×10^{-8} atm) that chromium volatilisation is negligible.

Reaction products were analysed by X-ray diffraction (XRD) using a Phillips X'pert Pro MPD diffractometer. Imaging and chemical analysis were carried out by optical microscopy (OM) and scanning electron microscopy combined with energy-dispersive X-ray spectroscopy (SEM-EDS), using a LEO 435VP microscope with PGT IMIX EDS system. Raman spectroscopy was performed using a Horiba Jobin–Yvon Labram HR 800 Raman microscope with an argon laser (wavelength 532 nm, power 20 mW), with a spatial resolution of 1 μm. The spectra of oxide phases in the Fe–Cr–O system were interpreted using the work of McCarty and Boehme [21], who studied Raman signatures of the spinel – ($Fe_{3-x}Cr_xO_4$) and corundum-type ($Fe_{2-x}Cr_xO_3$) solid solutions. The spectral resolution was 0.4 cm^{-1}, which allowed the oxide composition to be determined in a semi-quantitative way [21]. Metallographic observations were carried out on polished and etched cross-sections. Etching with Murakami's reagent (1 g $K_3Fe(CN)_6$ and 1 g KOH in 10 mL H_2O) revealed carbides.

3. Results

3.1. Overview

Exposure of Fe–20Cr, Fe–20Cr–10Ni, Fe–20Cr–20Ni and Fe–25Cr to dry and wet CO_2 resulted in non-uniform oxidation morphologies, as the alloys produced both a thin oxide scale and thicker oxide nodules characteristic of breakaway (Fig. 1). In contrast, Fe–25Cr–10Ni and Fe–25Cr–20Ni suffered no breakaway oxidation within the duration of the experiments, forming mainly a thin protective scale.

Total weight gains and surface fractions of nodular oxide varied considerably; the effects of alloy and gas composition on the kinetics of breakaway oxidation are reported in a companion paper [22].

3.2. Reaction products

After reaction in both dry and wet CO_2, analysis by XRD of oxidised specimen surfaces revealed the presence of Cr_2O_3 as the only oxide in the case of Fe–25Cr–10Ni and Fe–25Cr–20Ni. Optical microscope examination of the specimen surfaces revealed the presence of isolated nodules, 1–30 μm large. The nodules covered a very small fraction of the surface area, and only the thin chromia scale was seen in metallographic cross-sections. After reaction of all other alloys in dry and wet CO_2, Cr_2O_3, Fe_2O_3 and Fe_3O_4 were detected by XRD. Individual nodules approximately circular in plan (Fig. 1) and elliptical in cross-section (Fig. 2), and extensive areas of iron oxide formation were observed, along with regions of protective chromia scale.

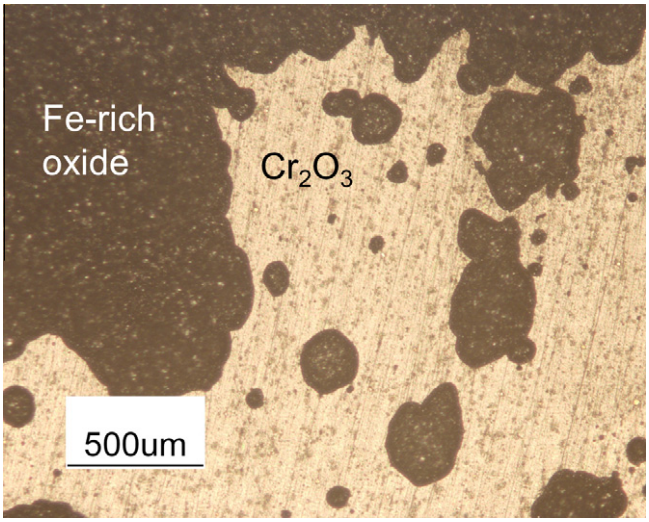

Fig. 1. Surface view of Fe–20Cr after 120 h reaction in Ar–20CO_2.

3.2.1. Fe–20Cr

During exposure to dry CO_2, the Fe–20Cr alloy produced a thin protective oxide scale and multilayer nodules, either isolated or forming semi-continuous scales of uniform thickness (Fig. 2). The only difference observed after exposure to Ar–20CO_2–5H_2O and Ar–20CO_2–20H_2O was that the extent of nodule formation was greater than in the dry gas, such that a multilayer scale of uniform thickness was observed on most of the cross-sections. Nodules appeared to be randomly distributed; in particular, nodule formation was not more important on the specimen edges than on the faces

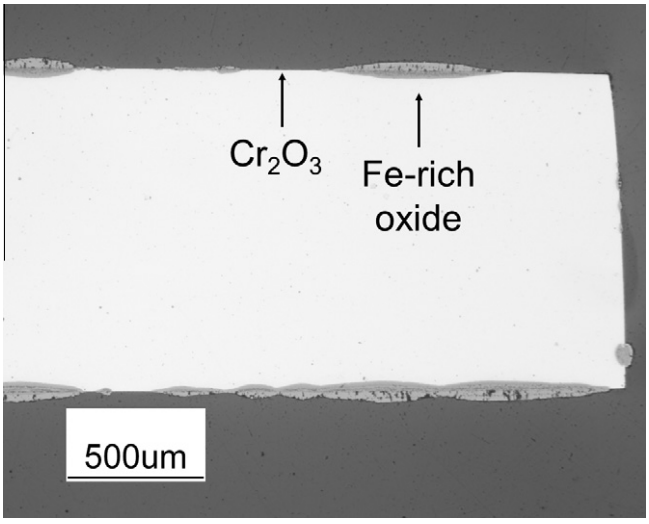

Fig. 2. Optical microscope overview of oxidation products grown on Fe–20Cr after 80 h reaction in Ar–20CO_2.